A Buck and Boost Based Grid Connected PV Inverter Maximizing Power Yield From Two PV Arrays in Mismatched Environmental Conditions

Subhendu Dutta and Kishore Chatterjee, *Member, IEEE*

***Abstract*—A single phase grid connected transformerless photovoltaic (PV) inverter, which can operate either in buck or in boost mode, and can extract maximum power simultaneously from two serially connected subarrays while each of the subarray is facing different environmental conditions, is presented in this paper. As the inverter can operate in buck as well as in boost mode, depending on the requirement, the constraint on the minimum number of serially connected solar PV modules that is required to form a subarray is greatly reduced. As a result, power yield from each of the subarray increases when they are exposed to different environmental conditions. The topological configuration of the inverter and its control strategy are designed so that the high-frequency components are not present in the common mode voltage, thereby restricting the magnitude of the leakage current associated with the PV arrays within the specified limit. Further, high operating efficiency is achieved throughout its operating range. A detailed analysis of the system leading to the development of its mathematical model is carried out. The viability of the scheme is confirmed by performing detailed simulation studies. A 1.5 kW laboratory prototype is developed, and detailed experimental studies are carried out to corroborate the validity of the scheme.**

***Index Terms*—Buck and Boost based photovoltaic (PV) inverter, grid connection, maximum power point (MPP), mismatched environmental condition, series connected module, single phase, transformerless.**

I. Introduction

THE major concern of a photovoltaic (PV) system is to ensure optimum performance of individual PV modules in a PV array while the modules are exposed to different environmental conditions arising due to difference in insolation level and/or difference in operating temperature. The presence of mismatch in operating condition of modules significantly reduces the power output from the PV array [1]. The problem with the mismatched environmental conditions (MECs) becomes significant if the number of modules connected in series in a PV array is large. In order to achieve desired magnitude for the input dc-link voltage of the inverter of a grid connected transformerless (GCT) PV system, the requirement of series connected modules becomes high. Therefore, the power output from a GCT PV system such as single phase GCT (SPGCT) inverter based systems derived from H-bridge [2], [3] and neutral point clamp (NPC) inverter based systems [4], [5] get affected significantly during MEC.

In order to address the problem arising out of MEC in a PV system, various solutions are reported in the literature. An exhaustive investigation of such techniques has been presented in [6]. Power extraction during MEC can be increased by choosing proper interconnection between PV modules [6], [7] or by tracking global maximum power point (MPP) of PV array by employing complex MPP tracking (MPPT) algorithm [6], [8]. However, these techniques are not effective for low power SPGCT PV system. Similarly, reconfiguration of the PV modules in a PV array by changing the electrical connection of PV modules [9], [10] is not effective for SPGCT PV system due to the considerable increment in component count and escalation in operating complexity. In order to extract maximum power from each PV module during MEC, attempts have been made to control each PV module in a PV array either by having a power electronic equalizer [11] or by interfacing a dc to dc converter [1], [12]–[14]. Schemes utilizing power electronic equalizer require large component count thereby increasing the cost and operation complexity of the system. The scheme presented in [1] uses generation control circuit (GCC) to operate each PV module at their respective MPP wherein the difference in power between each module is only processed through the GCC. Scheme presented in [12] uses shunt current compensation of each module as well as series voltage compensation of each PV string in a PV array to enhance power yield during MEC. The schemes based on module integrated converter [13], [14] use dedicated dc to dc converter integrated with each PV module. However, the efficiency of the aforesaid schemes are low due to the involvement of large number of converter stages, and further in these schemes the component count is high, and hence, they face similar limitations as that of power electronic equalizer based scheme. Instead of ensuring MPP operation of each and every module, certain number of modules are connected in series to form a string and the so formed strings are then made to operate under MPP in [15] and [16]. Even then,

Manuscript received July 12, 2017; revised October 10, 2017; accepted October 31, 2017. Date of publication November 17, 2017; date of current version March 6, 2018. *(Corresponding author: Subhendu Dutta.)*

The authors are with the Department of Electrical Engineering, Indian Institute of Technology Bombay, Mumbai 400076, India (e-mail: subdut87@gmail.com; kishore@ee.iitb.ac.in).

Color versions of one or more of the figures in this paper are available online at http://ieeexplore.ieee.org.

Digital Object Identifier 10.1109/TIE.2017.2774768

there is not much reduction in overall component count and control complexity [6].

In order to simplify the control configuration and to reduce the component count, schemes reported in [17] and [18] combine all the PV modules into two subarrays, and then, each of the subarrays is made to operate at their respective MPP. However, the reported overall efficiency of both the schemes are poor. By introducing a buck and boost stage in SPGCT PV inverter, power extraction during MEC is improved in [19]–[21]. Further, as a consequence of the presence of the intermediate boost stage, the requirement of series connected PV modules in a PV array has become less. In the schemes presented in [19]–[21], the switches of either the dc to dc converter stage or inverter stage operate at high frequency, as a result there is a considerable reduction in the size of the passive element count, thereby improving the operating efficiency of these schemes. Further, the reported efficiency of [20] and [21] is 1–2% higher than that of [19].

An effort has been made in this paper to divide the PV modules into two serially connected subarrays and controlling each of the subarray by means of a buck and boost based inverter so that optimum power evacuation from the subarrays is ascertained during MEC. This process of segregation of input PV array into two subarrays reduces the number of series connected modules in a subarray almost by half compared to that of the schemes proposed in [20] and [21]. The topological structure and control strategy of the proposed inverter ensure that the magnitude of leakage current associated with the PV arrays remains within the permissible limit. Further, the voltage stress across the active devices is reduced almost by half compared to that of the schemes presented in [20] and [21]; hence, very high-frequency operation without increasing the switching loss is ensured. High-frequency operation also leads to the reduction in the size of the passive elements. As a result the operating efficiency of the proposed scheme is high. The measured peak efficiency and the European efficiency (η_{euro}) of the proposed scheme is found to be 97.65% and 97.02%, respectively.

The detailed operation of the proposed inverter with mathematical validation is explained in Section II. Afterwards the mathematical model of the proposed inverter has been derived in Section III followed by the philosophy of control strategy in Section IV. The criteria to select the values of the output filter components are presented in Section V. The proposed scheme is verified by performing extensive simulation studies and the simulated performance is presented in Section VI. A 1.5 kW laboratory prototype of the proposed inverter has been fabricated to carry out thorough experimental studies. The measured performances of the scheme, which confirm its viability are presented in Section VII.

II. Proposed Inverter and its Operation

The schematic of the proposed dual buck and boost based inverter (DBBI), which is depicted in Fig. 1, is comprised of a dc to dc converter stage followed by an inverting stage. The dc to dc converter stage has two dc to dc converter segments, CONV_1 and CONV_2 to service the two subarrays: PV_1 and PV_2 of the solar PV array. The segment CONV_1 consists of the

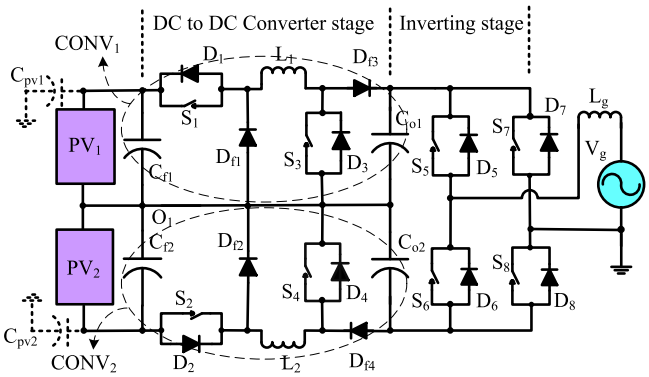

Fig. 1. Dual buck and boost based Inverter.

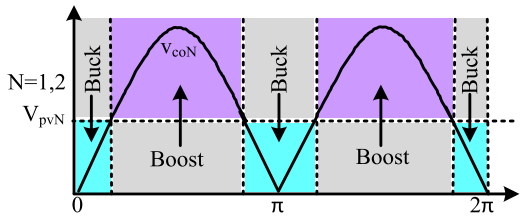

Fig. 2. Buck stage and boost stage of the proposed inverter.

self-commutated switches, S_1 along with its antiparallel body diode D_1, S_3 along with its antiparallel body diode D_3, the free wheeling diodes D_{f1}, D_{f3}, and the filter inductors and capacitors L_1, C_{f1}, and C_{o1}. Similarly, the segment, CONV_2 consists of the self-commutated switches, S_2 along with its antiparallel body diode D_2, S_4 along with its antiparallel body diode D_4, the free wheeling diodes D_{f2}, D_{f4}, and the filter inductors and capacitors L_2, C_{f2}, and C_{o2}. The inverting stage is consisting of the self-commutated switches S_5, S_6, S_7, S_8 and their corresponding body diodes D_5, D_6, D_7, and D_8, respectively. The inverter stage is interfaced with the grid through the filter inductor, L_g. The PV array to the ground parasitic capacitance is modeled by the two capacitors C_{pv1} and C_{pv2}.

Considering Fig. 2, CONV_1 operates in buck mode when $V_{\text{pv1}} \geq v_{\text{co1}}$, while CONV_2 operates in buck mode when $V_{\text{pv2}} \geq v_{\text{co2}}$. V_{pv1}, V_{pv2} are the MPP voltages of PV_1 and PV_2 and v_{co1}, v_{co2} are the output voltages of CONV_1 and CONV_2, respectively. During buck mode duty ratios of the switches, S_1 and S_2 are varied sinusoidally to ensure sinusoidal grid current (i_g) while S_3 and S_4 are kept OFF. When $V_{\text{pv1}} < v_{\text{co1}}$, CONV_1 operates in boost mode while CONV_2 operates in boost mode when $V_{\text{pv2}} < v_{\text{co2}}$. During boost mode duty ratios of the switches, S_3 and S_4 are varied sinusoidally to ensure sinusoidal i_g while S_1 and S_2 are kept on throughout this mode. The sinusoidal switching pulses of the switches of CONV_1 and CONV_2 are synchronized with the grid voltage, v_g to accomplish unity power factor operation. The switches S_5 and S_8 are kept ON, and switches S_6 and S_7 are kept OFF permanently during the entire positive half-cycle (PHC) while during entire negative half-cycle (NHC), the switches, S_6 and S_7 are kept ON and switches, S_5 and S_8 are kept OFF permanently. All the operating states of the proposed inverter are depicted in Fig. 3.

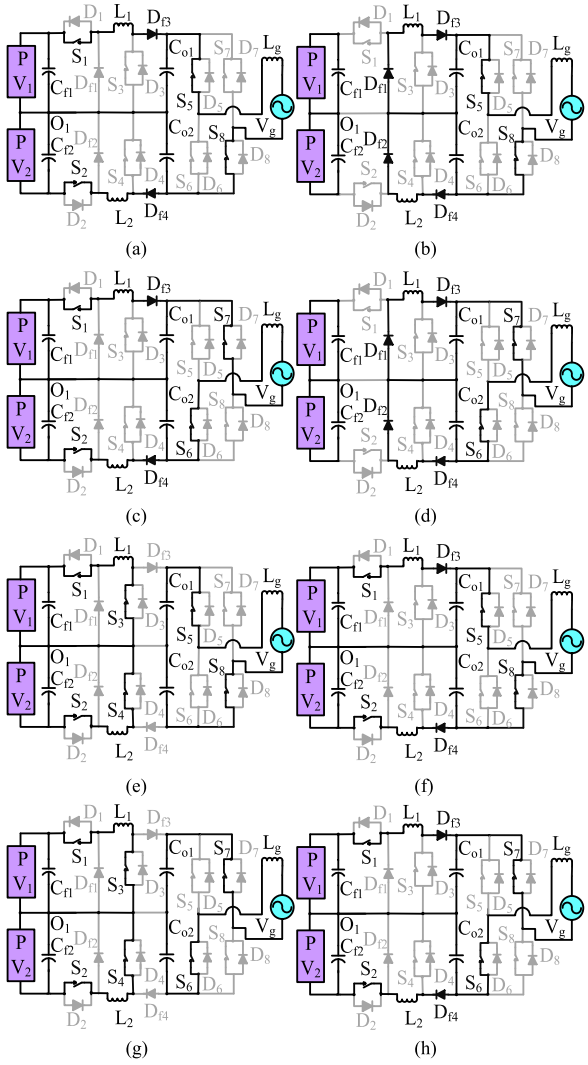

Fig. 3. Operating states of DBBI. (a) Active and (b) freewheeling states in buck mode of PHC, (c) active and (d) freewheeling states in buck mode of NHC, (e) active and (f) freewheeling states in boost mode of PHC, and (g) active and (h) freewheeling states in boost mode of NHC.

When the insolation level and ambient temperature of subarray PV_1 are different from that of PV_2, the MPP parameters of the two subarrays V_{pv1} and V_{pv2}, MPP current I_{pv1} and I_{pv2} correspond to PV_1 and PV_2, respectively, and power at MPP P_{pv1} and P_{pv2} correspond to PV_1 and PV_2, respectively, differ from each other. By considering that both the subarrays are operating at their respective MPP and neglecting the losses incurred in power processing stages, the average power involved with C_{o1} and C_{o2}, P_{co1} and P_{co2} over a half-cycle can be assumed equal to the power extracted from PV_1 and PV_2. Therefore

$$P_{\mathrm{co1}} = P_{\mathrm{pv1}} \quad \text{and} \quad P_{\mathrm{co2}} = P_{\mathrm{pv2}}. \tag{1}$$

The power injected to the grid averaged over a half-cycle, P_g can be written as

$$P_g = P_{\mathrm{pv1}} + P_{\mathrm{pv2}}. \tag{2}$$

Further, at any half-cycle

$$v_g = v_{\mathrm{co1}} + v_{\mathrm{co2}}. \tag{3}$$

Hence, the instantaneous injected power to the grid, p_g can be written as

$$p_g = v_g i_g = (v_{\mathrm{co1}} + v_{\mathrm{co2}}) i_g \tag{4}$$

wherein v_{co1} and v_{co2} denote the instantaneous quantities of V_{co1} and V_{co2}, respectively. As i_g is in-phase with v_g

$$I_g = \frac{P_g}{V_g} \tag{5}$$

wherein V_g and I_g denote rms values of v_g and i_g, respectively. The power injected to the grid can be expressed as

$$\begin{aligned} P_g &= \frac{1}{\pi}\int_0^{\pi} p_g \, d(\omega t) \\ &= \frac{1}{\pi}\int_0^{\pi} v_{\mathrm{co1}} i_g \, d(\omega t) + \frac{1}{\pi}\int_0^{\pi} v_{\mathrm{co2}} i_g \, d(\omega t) \qquad (6) \\ &= P_{\mathrm{co1}} + P_{\mathrm{co2}}. \qquad (7) \end{aligned}$$

As v_{co1} and v_{co2} are synchronized with v_g. Hence

$$\begin{aligned} P_{\mathrm{co1}} &= \frac{1}{\pi}\int_0^{\pi} V_{\mathrm{co1}m} \sin(\omega t)\, I_{gm} \sin(\omega t)\, d(\omega t) \\ &= \frac{V_{\mathrm{co1}m} I_{gm}}{2}. \qquad (8) \end{aligned}$$

Similarly

$$P_{\mathrm{co2}} = \frac{V_{\mathrm{co2}m} I_{gm}}{2} \tag{9}$$

wherein the amplitudes of $v_{\mathrm{co1}}, v_{\mathrm{co2}}$, and i_g are denoted as $V_{\mathrm{co1}m}, V_{\mathrm{co2}m}$, and I_{gm}, respectively. Combining (1), (8), and (9)

$$V_{\mathrm{co1}m} = \frac{2P_{\mathrm{pv1}}}{I_{gm}} = \frac{\sqrt{2}P_{\mathrm{pv1}}}{I_g} = \frac{\sqrt{2}P_{\mathrm{pv1}}}{P_g/V_g} \tag{10}$$

$$V_{\mathrm{co2}m} = \frac{2P_{\mathrm{pv2}}}{I_{gm}} = \frac{\sqrt{2}P_{\mathrm{pv2}}}{I_g} = \frac{\sqrt{2}P_{\mathrm{pv2}}}{P_g/V_g}. \tag{11}$$

Similarly by combining (2), (10), and (11)

$$V_{\mathrm{co1}m} = \frac{V_m P_{\mathrm{pv1}}}{P_{\mathrm{pv1}} + P_{\mathrm{pv2}}} \quad \text{and} \quad V_{\mathrm{co2}m} = \frac{V_m P_{\mathrm{pv2}}}{P_{\mathrm{pv1}} + P_{\mathrm{pv2}}}. \tag{12}$$

The voltage templates of v_{co1} and v_{co2} appear as full wave rectified sinusoidal waveform with amplitudes, $V_{\mathrm{co1}m}$ and $V_{\mathrm{co2}m}$, respectively. V_m is the amplitude of v_g. It can be deduced from (12) that the magnitudes of $V_{\mathrm{co1}m}$ and $V_{\mathrm{co2}m}$ are decided by the power extracted from each of the subarray. If the power extracted from PV_1 is less than PV_2, then $V_{\mathrm{co1}m} < V_{\mathrm{co2}m}$, whereas $V_{\mathrm{co2}m} < V_{\mathrm{co1}m}$ if power extracted from PV_2 is less than PV_1. During buck mode, the duty ratios, d_1 of S_1 and d_2 of S_2 vary sinusoidally with an amplitude d_{1m} and d_{2m}, wherein

$$d_{1m} = \frac{V_{\mathrm{co1}m}}{V_{\mathrm{pv1}}} \quad \text{and} \quad d_{2m} = \frac{V_{\mathrm{co2}m}}{V_{\mathrm{pv2}}} \tag{13}$$

while during boost mode the duty ratios, d_3 of S_3 and d_4 of S_4 vary sinusoidally with amplitude d_{3m} and d_{4m}, wherein

$$d_{3m} = 1 - \frac{V_{\mathrm{pv1}}}{V_{\mathrm{co1}m}} \quad \text{and} \quad d_{4m} = 1 - \frac{V_{\mathrm{pv2}}}{V_{\mathrm{co2}m}}. \tag{14}$$

The CONV_1 and CONV_2 have the same output current i_g. Hence, the input side currents before getting filtered by input filter capacitors of CONV_1, i_{sw1} and CONV_2, i_{sw2} can be related with i_g in the buck mode by considering the switching cycle average of corresponding quantities as follows:

$$\langle i_{\text{sw1}}\rangle_{T_s} = \langle d_1\rangle_{T_s}\langle i_g\rangle_{T_s} \tag{15}$$

$$\langle i_{\text{sw2}}\rangle_{T_s} = \langle d_2\rangle_{T_s}\langle i_g\rangle_{T_s}. \tag{16}$$

Similarly by considering switching cycle average of corresponding quantities the relation between i_{sw1}, i_{sw2}, and i_g can be deduced during boost mode as

$$\langle i_{\text{sw1}}\rangle_{T_s} = \left\langle \frac{1}{1-d_3}\right\rangle_{T_s}\langle i_g\rangle_{T_s} \tag{17}$$

$$\langle i_{\text{sw2}}\rangle_{T_s} = \left\langle \frac{1}{1-d_4}\right\rangle_{T_s}\langle i_g\rangle_{T_s}. \tag{18}$$

Therefore, it can be inferred from (12) and (13) that if the insolation level of PV_1 is lower than that of PV_2, during buck mode, $d_{1m} < d_{2m}$, thereby $\langle d_1\rangle_{T_s} < \langle d_2\rangle_{T_s}$ whereas during boost mode as per (12) and (14), $d_{3m} < d_{4m}$, thereby $\langle d_3\rangle_{T_s} < \langle d_4\rangle_{T_s}$. Hence, it can be concluded from (15)–(17), and (18) that in any operating mode, $\langle i_{\text{sw1}}\rangle_{T_s} < \langle i_{\text{sw2}}\rangle_{T_s}$; therefore, $I_{\text{pv1}} < I_{\text{pv2}}$. Following the same argument, $I_{\text{pv1}} > I_{\text{pv2}}$ if the insolation level of PV_1 is higher than that of PV_2.

Considering Fig. 1 it can be noted that during operation in PHC, $v_{\text{cpv1}} = v_{\text{co2}} + V_{\text{pv1}}$, $v_{\text{cpv2}} = v_{\text{co2}} - V_{\text{pv2}}$ while during NHC $v_{\text{cpv1}} = -v_{\text{co1}} + V_{\text{pv1}}, v_{\text{cpv2}} = -v_{\text{co1}} - V_{\text{pv2}}$, wherein v_{cpv1} and v_{cpv2} are the voltages impressed across C_{pv1} and C_{pv2}, respectively. Hence, the voltages across C_{pv1} and C_{pv2} contain significant amount of dc and low-frequency components, which also ensures that the magnitude of the leakage current is maintained within the limit specified in the standard VDE 0126-1-1, and also cited in [23].

III. Mathematical Model of the Proposed Scheme

A small signal modeling of the proposed inverter has been carried out for buck mode and boost mode of operation. Fig. 4(a) and (b) represent the equivalent circuit of the proposed inverter while it operates in buck mode, whereas Fig. 4(c) and (d) represent the equivalent circuit of the converter while it operates in boost mode. R_{L1}, R_{L2}, R_g, R_{co1}, and R_{co2} are the parasitic resistances of L_1, L_2, L_g, C_{o1}, and C_{o2}, respectively. As indirect grid current control method [21] is adopted to control i_g, the quantities i_{L1}, i_{L2}, v_{co1}, v_{co2}, and i_g are considered to be the state variables. The state equations representing the buck mode of operation of the inverter are derived to be (19) and (20), shown at the bottom of the next page, by considering the equivalent circuits of Fig. 4(a) and (b), while the state equations for boost mode are derived to be (21) and (19), also shown at the bottom of the next page, by considering the equivalent circuits of Fig. 4(c) and (d).

The state-space averaging based technique is adopted as the grid frequency, f_g is adequately lower than the switching frequency, f_s. In order to simplify the analysis, V_{pv1}, V_{pv2}, and v_g are considered as stiff voltage sources, and the effect of input

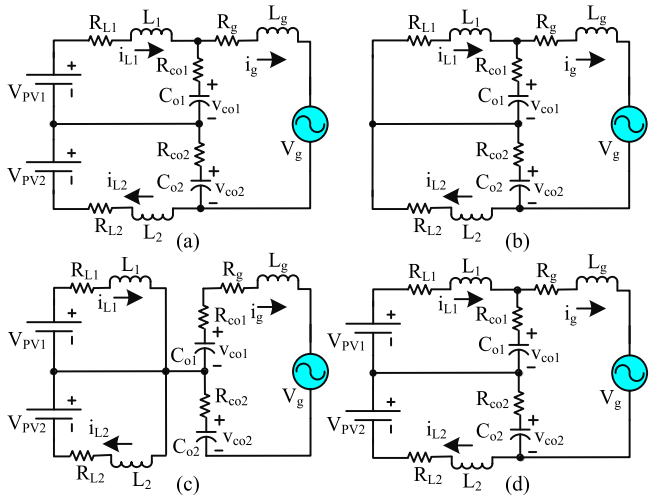

Fig. 4. Equivalent circuit in buck mode (a) S_1, S_2 are ON, (b) S_1, S_2 are OFF in boost mode, (c) S_3, S_4 are ON, and (d) S_3, S_4 are OFF.

filter capacitors is neglected. The values of the system parameters are considered to be as follows: $R_{L1} = R_{L2} = 0.12\ \Omega$, $R_g = 0.04\ \Omega$, $R_{\text{co1}} = R_{\text{co2}} = 0.26\ \Omega$, $V_{\text{pv1}} = V_{\text{pv2}} = 130$ V. Considering symmetry in operation of CONV_1 and CONV_2, and by applying state-space averaging technique to (19)–(21), the simplified transfer functions of $i_g(s)/d(s)$, $i_{L1}(s)/d(s)$, and $v_{\text{co1}}(s)/d(s)$ in s-domain during buck mode are obtained as

$$\frac{i_g(s)}{d(s)} = \frac{2.87\times10^8 s + 2.2\times10^{14}}{s^3 + 2267\times s^2 + 1.33\times10^9 s + 3\times10^{11}} \tag{22}$$

$$\frac{i_{L1}(s)}{d(s)} = \frac{2.17\times10^5 s^2 + 3.52\times10^8 s + 2.2\times10^{14}}{s^3 + 2267\times s^2 + 1.33\times10^9 s + 3\times10^{11}} \tag{23}$$

$$\frac{v_{\text{co1}}(s)}{d(s)} = \frac{4.33\times10^{10} s + 1.3\times10^{13}}{s^3 + 2267\times s^2 + 1.33\times10^9 s + 3\times10^{11}} \tag{24}$$

where in d is the duty ratio of component converters. Similarly, the simplified transfer functions of $i_g(s)/d(s)$, $i_{L1}(s)/d(s)$, and $v_{\text{co1}}(s)/d(s)$ in s-domain during boost mode are obtained as

$$\frac{i_g(s)}{d(s)} = \frac{-9487 s^2 - 9.7\times10^9 s + 2.1\times10^{14}}{s^3 + 2018\times s^2 + 1.26\times10^9 s + 2.7\times10^{11}} \tag{25}$$

$$\frac{i_{L1}(s)}{d(s)} = \frac{2.4\times10^5 s^2 + 3.3\times10^9 s + 2.4\times10^{14}}{s^3 + 2018\times s^2 + 1.26\times10^9 s + 2.7\times10^{11}} \tag{26}$$

$$\frac{v_{\text{co1}}(s)}{d(s)} = \frac{-2\times10^6 s^2 + 4.1\times10^{10} s + 4\times10^{12}}{s^3 + 2018\times s^2 + 1.26\times10^9 s + 2.7\times10^{11}}. \tag{27}$$

Due to the existence of symmetry, transfer functions for $i_{L2}(s)/d(s)$ and $v_{\text{co2}}(s)/d(s)$ remain the same as that of (23), (24) in buck mode and (26) and (27) in boost mode, respec-

tively. Based on the derived transfer functions of the system, compensators are designed to achieve the phase margin of 90° for both the plants, and at the same time to maintain the desired total harmonic distortion (THD) for the grid current.

IV. Control Strategy of the Proposed Scheme

The control strategy of the proposed scheme is depicted in Fig. 5. The controller is designed to fulfill the following objectives.

1) Both subarrays operate at their corresponding MPP simultaneously.
2) Sensing of output voltages v_{co1} and v_{co2} is not required.
3) i_g is sinusoidal and is in-phase with v_g throughout the operating range.

Two separate MPP trackers and two proportional integral (PI) controllers are employed to determine the value of P_{pv1} and P_{pv2}, which are required to estimate V_{co1m} and V_{co2m}. Using (12), V_{co1m} and V_{co2m} are determined where the information of V_m is obtained from the phase locked loop (PLL). A rectified version of a unity sinusoidal function, R is generated from a unity sinusoidal function, X, synchronized with v_g, and is obtained from the same PLL. R is multiplied with V_{co1m} and V_{co2m} to estimate v_{co1} and v_{co2}. Hence, two voltage sensors

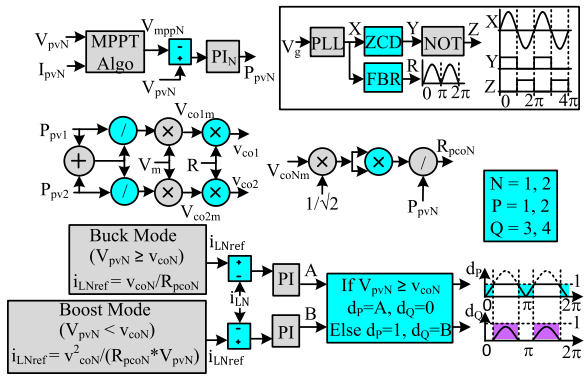

Fig. 5. Control configuration of the proposed inverter.

$$\begin{bmatrix} \dot{i}_{L1}(t) \\ \dot{i}_{L2}(t) \\ \dot{v}_{co1}(t) \\ \dot{v}_{co2}(t) \\ \dot{i}_g(t) \end{bmatrix} = \begin{bmatrix} -\frac{R_{L1}+R_{co1}}{L_1} & 0 & -\frac{1}{L_1} & 0 & \frac{R_{co1}}{L_1} \\ 0 & -\frac{R_{L2}+R_{co2}}{L_2} & 0 & -\frac{1}{L_2} & \frac{R_{co2}}{L_2} \\ \frac{1}{C_{o1}} & 0 & 0 & 0 & -\frac{1}{C_{o1}} \\ 0 & \frac{1}{C_{o2}} & 0 & 0 & -\frac{1}{C_{o2}} \\ \frac{R_{co1}}{L_g} & \frac{R_{co2}}{L_g} & \frac{1}{L_g} & \frac{1}{L_g} & -\frac{R_{co1}+R_{co2}+R_g}{L_g} \end{bmatrix} \begin{bmatrix} i_{L1}(t) \\ i_{L2}(t) \\ v_{co1}(t) \\ v_{co2}(t) \\ i_g(t) \end{bmatrix} + \begin{bmatrix} \frac{1}{L_1} & 0 & 0 \\ 0 & \frac{1}{L_2} & 0 \\ 0 & 0 & 0 \\ 0 & 0 & 0 \\ 0 & 0 & -\frac{1}{L_g} \end{bmatrix} \begin{bmatrix} v_{pv1}(t) \\ v_{pv2}(t) \\ v_g(t) \end{bmatrix} \tag{19}$$

$$\begin{bmatrix} \dot{i}_{L1}(t) \\ \dot{i}_{L2}(t) \\ \dot{v}_{co1}(t) \\ \dot{v}_{co2}(t) \\ \dot{i}_g(t) \end{bmatrix} = \begin{bmatrix} -\frac{R_{L1}+R_{co1}}{L_1} & 0 & -\frac{1}{L_1} & 0 & \frac{R_{co1}}{L_1} \\ 0 & -\frac{R_{L2}+R_{co2}}{L_2} & 0 & -\frac{1}{L_2} & \frac{R_{co2}}{L_2} \\ \frac{1}{C_{o1}} & 0 & 0 & 0 & -\frac{1}{C_{o1}} \\ 0 & \frac{1}{C_{o2}} & 0 & 0 & -\frac{1}{C_{o2}} \\ \frac{R_{co1}}{L_g} & \frac{R_{co2}}{L_g} & \frac{1}{L_g} & \frac{1}{L_g} & -\frac{R_{co1}+R_{co2}+R_g}{L_g} \end{bmatrix} \begin{bmatrix} i_{L1}(t) \\ i_{L2}(t) \\ v_{co1}(t) \\ v_{co2}(t) \\ i_g(t) \end{bmatrix} + \begin{bmatrix} 0 & 0 & 0 \\ 0 & 0 & 0 \\ 0 & 0 & 0 \\ 0 & 0 & 0 \\ 0 & 0 & -\frac{1}{L_g} \end{bmatrix} \begin{bmatrix} v_{pv1}(t) \\ v_{pv2}(t) \\ v_g(t) \end{bmatrix} \tag{20}$$

$$\begin{bmatrix} \dot{i}_{L1}(t) \\ \dot{i}_{L2}(t) \\ \dot{v}_{co1}(t) \\ \dot{v}_{co2}(t) \\ \dot{i}_g(t) \end{bmatrix} = \begin{bmatrix} -\frac{R_{L1}}{L_1} & 0 & 0 & 0 & 0 \\ 0 & -\frac{R_{L2}}{L_2} & 0 & 0 & 0 \\ 0 & 0 & 0 & 0 & -\frac{1}{C_{o1}} \\ 0 & 0 & 0 & 0 & -\frac{1}{C_{o2}} \\ 0 & 0 & \frac{1}{L_g} & \frac{1}{L_g} & -\frac{R_{co1}+R_{co2}+R_g}{L_g} \end{bmatrix} \begin{bmatrix} i_{L1}(t) \\ i_{L2}(t) \\ v_{co1}(t) \\ v_{co2}(t) \\ i_g(t) \end{bmatrix} + \begin{bmatrix} \frac{1}{L_1} & 0 & 0 \\ 0 & \frac{1}{L_2} & 0 \\ 0 & 0 & 0 \\ 0 & 0 & 0 \\ 0 & 0 & -\frac{1}{L_g} \end{bmatrix} \begin{bmatrix} v_{pv1}(t) \\ v_{pv2}(t) \\ v_g(t) \end{bmatrix}. \tag{21}$$

that otherwise would have been required to determine v_{co1} and v_{co2} get eliminated. V_{pv1} and v_{co1} are compared to decide about the mode of operation (buck mode or boost mode) of CONV$_1$, while V_{pv2} and v_{co2} are compared to determine the mode of operation of CONV$_2$. RMS values of v_{co1} and v_{co2} are estimated, which are then subsequently squared and are then divided by P_{pv1} and P_{pv2} to obtain the emulated effective resistances, R_{pco1} and R_{pco2} of the two component converters. Subsequently the reference current, i_{L1ref} of L_1, and the reference current, i_{L2ref} of L_2, are synthesized by utilizing (28) in the buck mode [21]

$$i_{L1ref} = \frac{v_{co1}}{R_{pco1}} \quad \text{and} \quad i_{L2ref} = \frac{v_{co2}}{R_{pco2}} \tag{28}$$

while for boost mode (29), it is used to generate i_{L1ref} and i_{L2ref} [21].

$$i_{L1ref} = \frac{v_{co1}^2}{R_{pco1} V_{pv1}} \quad \text{and} \quad i_{L2ref} = \frac{v_{co2}^2}{R_{pco2} V_{pv2}}. \tag{29}$$

The sensed inductor currents, i_{L1} and i_{L2} are compared with their corresponding references i_{L1ref} and i_{L2ref}. The errors so obtained are processed through two separate PI controllers to generate the required sinusoidal duty ratios for the switches, S_1 and S_2 during buck mode. Similarly, two separate PI controllers are engaged to process the generated errors to synthesize required sinusoidal duty ratios for switches S_3 and S_4 during boost mode. Signal Y is used to generate gating signals for S_5, S_8 while signal Z is used to generate gating signals for S_6, S_7 of the grid frequency unfolding inverter.

V. Selection of L_1, L_2, L_g, and C_{o1}, C_{o2}

In order to select the value of the filter elements, L_1, L_2, L_g, and C_{o1}, C_{o2} the design principle given in [24] is followed and the buck mode of operation for the inverter is considered. Values of L_1 and L_2 are obtained from the expression given in [24]

$$L_1 = \frac{V_{pv1}}{4\Delta I_{L1} f_s} \quad \text{and} \quad L_2 = \frac{V_{pv2}}{4\Delta I_{L2} f_s} \tag{30}$$

where in $V_{pv1} = V_{pv2} = 200$ V, and percentage peak to peak ripple of i_{L1} and i_{L2}, ΔI_{L1} and ΔI_{L2} are considered as 15% of rated peak current.

The values of C_{o1} and C_{o2} are obtained from the expression given in [24]

$$C_{o1} = \frac{xP_{co1}}{2\pi f_g V_{co1}^2} \quad \text{and} \quad C_{o2} = \frac{xP_{co2}}{2\pi f_g V_{co2}^2} \tag{31}$$

where in $V_{co1} = V_{co2} = 110$ V, $P_{co1} = P_{co2} = 750$ W, and factor $x = 2.5\%$.

In order to achieve wide stability margin and large control bandwidth a value, which is less than L_1 or L_2 is selected for L_g [24].

VI. Simulation Study

To demonstrate the efficacy of the proposed inverter a PV array consisting of two PV subarrays while each of the subarray having four series connected Canadian solar polycrystalline modules "CS6P-165PE" [25] is considered. The MPP parameters of each subarray at standard test condition (STC) are as follows: $V_{pv1} = V_{pv2} = 116$ V, $I_{pv1} = I_{pv2} = 5.7$ A, and $P_{pv1} = P_{pv2} = 661$ W. The parameters that are used to simulate the proposed inverter are indicated in Table I. MATLAB-Simulink platform is utilized to simulate the performance of the proposed inverter.

TABLE I
Employed Parameters/Elements for Simulation and Experimental Purpose

Parameter/elements	Value
V_g and f_g	220 V and 50 Hz
L_1, L_2, L_g, and C_{o1}, C_{o2}	0.6 mH, 0.6 mH, 0.4 mH, and 5 μF, 5 μF
C_{pv1} and C_{pv2}	0.1 μF
MPPT Algorithm	Incremental Conductance
MOSFETS (S_1–S_8)	IPW60R041C6
Diodes (D_{f1}–D_{f4})	MBR40250
f_s of S_1–S_4 and f_s of S_5–S_8	50 kHz and 50 Hz
Digital signal controller	TMS320F28335

TABLE II
Estimated Variations of Different Quantities During Applied Variations on Insolation and Temperature of Two Subarrays

Time in Second	0–1	1–2	2–3	3–4	4–5	5–6	6–7	7–8
Insol. in PV$_1$ (kW/m^2)	0.5	0.6	0.7	0.8	0.9	1.0	1.0	1.0
Insol. in PV$_2$ (kW/m^2)	0.8	0.8	0.8	0.8	0.8	0.8	0.8	0.8
Temp. in PV$_1$ (°C)	25	25	25	25	25	25	30	35
Temp. in PV$_2$ (°C)	25	25	25	25	25	25	25	25
P_{pv1} (W)	331	397	463	529	595	661	638	621
P_{pv2} (W)	529	529	529	529	529	529	529	529
I_{gm} (A)	5.5	6.0	6.4	6.8	7.2	7.7	7.5	7.4
V_{co1m} (V)	120	133	147	155	165	173	170	168
V_{co2m} (V)	191	178	164	156	146	138	141	143
I_{L1m} (A)	5.7	7	8.1	9	10.3	11.4	11	10.7
I_{L2m} (A)	9	9	9	9	9	9	9	9

The variation in insolation level and temperature with respect to time, which is considered for the two subarrays to demonstrate the effectiveness of the proposed inverter are tabulated in Table II. Estimated variation of P_{pv1}, P_{pv2} along with the other parameters I_{gm}, V_{co1m}, V_{co2m}, peak of i_{L1} (I_{L1m}) and peak of i_{L2} (I_{L2m}) are also indicated in the same table. Fig. 6(a)–(c) represents the variation of P_{pv1}, P_{pv2}, V_{pv1}, V_{pv2}, I_{pv1}, I_{pv2} of the two subarrays and also demonstrate the ability of the proposed inverter to operate the two subarrays simultaneously at their respective MPP. Variation in i_g, i_{L1}, i_{L2}, v_{co1}, and v_{co2} along with their magnified versions for two different insolation levels are depicted in Figs. 7–9. The estimated values of the aforementioned quantities as tabulated in Table II conform to that of obtained through simulation studies, thereby ensuring the viability of the proposed scheme.

VII. Experimental Verification

A 1.5 kW laboratory prototype of the proposed inverter is fabricated and detailed experimental studies have been carried out to demonstrate the effectiveness of the proposed scheme. The parameters as mentioned in Table I are used to realize the laboratory prototype of the inverter. In order to realize PV$_1$ and PV$_2$ two programmable EPS PSI9360-15 power supplies having

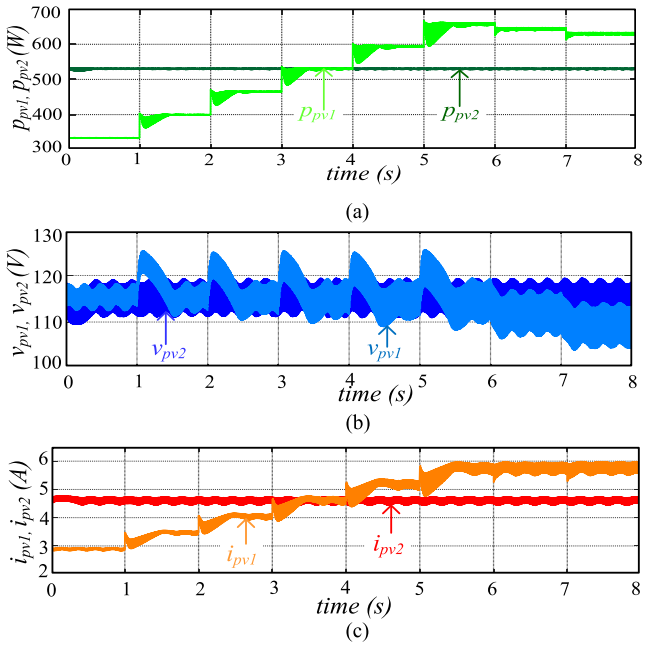

Fig. 6. Simulated waveform. Variation in (a) p_{pv1} and p_{pv2}, (b) v_{pv1} and v_{pv2}, and (c) i_{pv1} and i_{pv2} during entire range of operation.

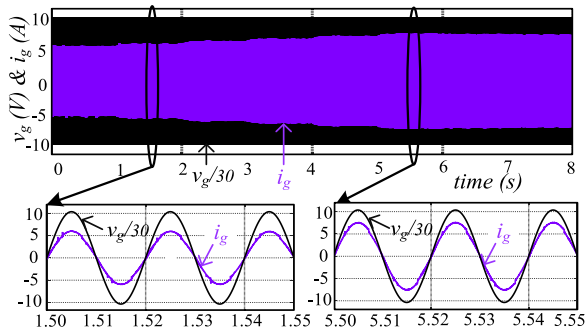

Fig. 7. Simulated waveform. v_g and i_g and their magnified views.

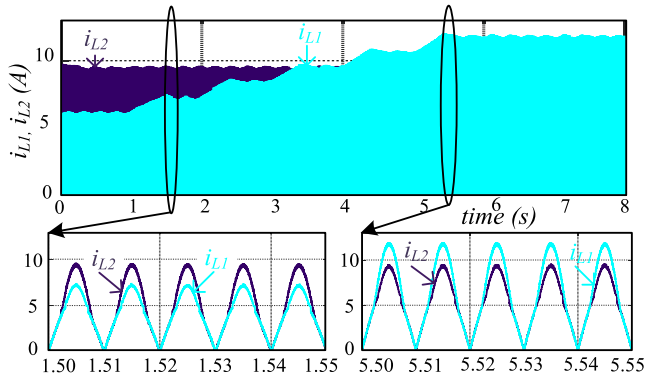

Fig. 8. Simulated waveform. i_{L1} and i_{L2} and their magnified views.

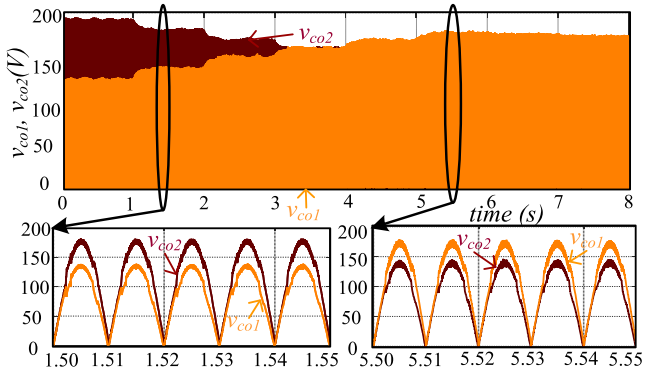

Fig. 9. Simulated waveform. v_{co1} and v_{co2} and their magnified views.

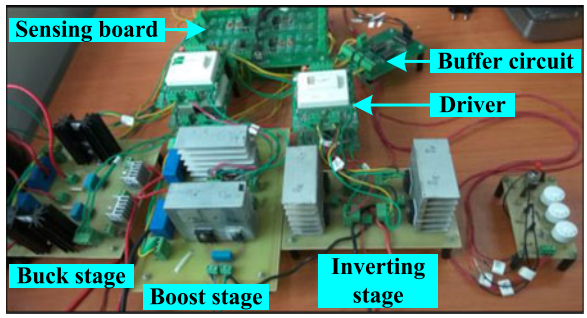

Fig. 10. Experimental prototype of the proposed inverter.

solar PV emulation feature are utilized. The photograph of the experimental prototype is shown in Fig. 10.

The EPS PSI9306-15 power supply has the provision to change only the effect of insolation level while the option to change the effect of temperature is unavailable. In order to emulate simultaneous variation in temperature and level of insolation, the MPP parameters of the two solar emulators (solar emulator 1 as PV_1 and solar emulator 2 as PV_2) are set as follows at STC: $V_{pv1} = 130$ V, $I_{pv1} = 5$ A, and $V_{pv2} = 120$ V, $I_{pv2} = 5$ A. The variation in insolation level of PV_1 is indicated in Table III while the insolation level of PV_2 is maintained at 80%. The expected values of $I_{pv1}, I_{pv2}, P_{pv1}, P_{pv2}, V_{co1m}, V_{co2m}, I_{gm}$, I_{L1m}, and I_{L2m} for the entire operating range are tabulated in the Table III. Fig. 11 depicts the change in i_g, I_{pv1}, I_{pv2}, P_{pv1}, and P_{pv2} throughout the range of variation in the level of insolation as specified in Table III. Magnified version of the responses of v_{co1}, v_{co2}, i_{L1}, and i_{L2}, along with v_g, i_g, are also shown in Fig. 12(a)–(f) for two different insolation levels of PV_1. The

TABLE III
ESTIMATED VARIATION IN $I_{pv1}, I_{pv2}, P_{pv1}, P_{pv2}, V_{co1m}, V_{co2m}, I_{gm}, I_{L1m}, I_{L2m}$ DURING PV_1 INSOLATION VARIATION

% Insol. of PV_1	40	50	60	70	80	90	100
% Insol. of PV_2	80	80	80	80	80	80	80
I_{pv1} (A)	2	2.5	3	3.5	4	4.5	5
I_{pv2} (A)	4	4	4	4	4	4	4
P_{pv1} (W)	260	325	390	455	520	585	650
P_{pv2} (W)	480	480	480	480	480	480	480
V_{co1m} (V)	109	126	140	151	162	171	179
V_{co2m} (V)	202	185	171	160	149	140	132
I_{gm} (A)	4.6	5	5.4	5.8	6.2	6.6	7
I_{L1m} (A)	4.6	5	5.8	6.8	7.8	8.7	10
I_{L2m} (A)	7.7	7.7	7.7	7.7	7.7	7.7	7.7

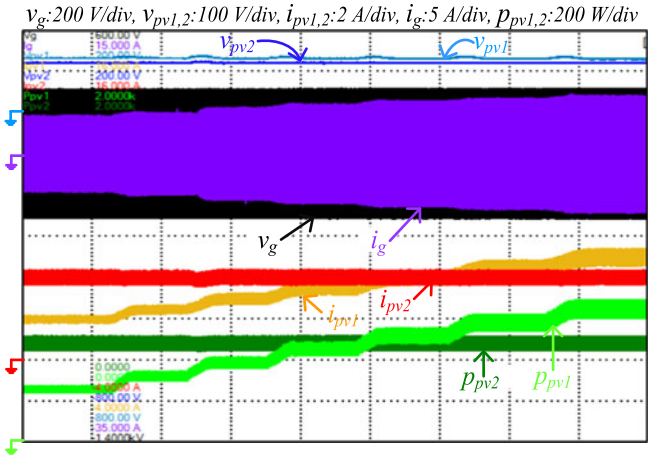

Fig. 11. Experimental waveforms. v_{pv1}, v_{pv2}, i_g, v_g, i_{pv1}, i_{pv2}, p_{pv1}, and p_{pv2} throughout the entire operating range.

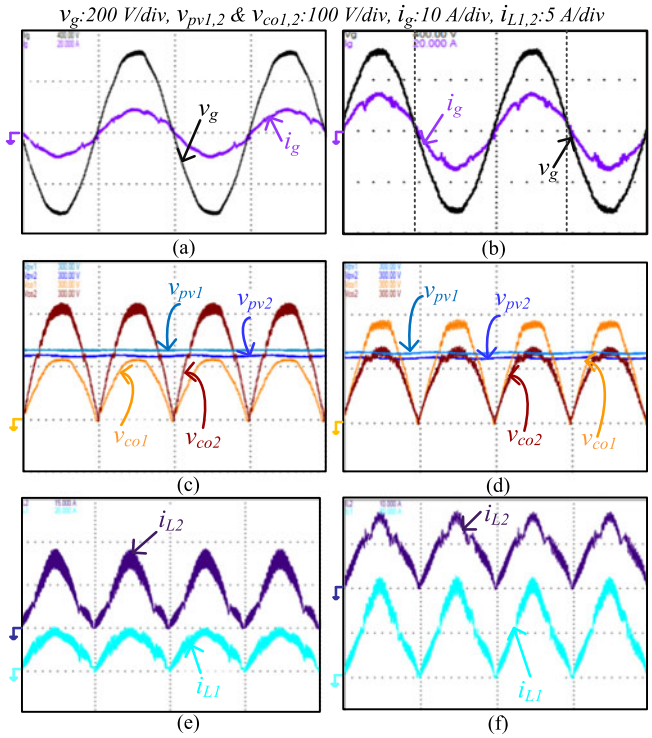

Fig. 12. Experimental waveforms. Magnified version of i_g, v_g when (a) insolation of $\text{PV}_1 = 40\%$ and insolation of $\text{PV}_2 = 80\%$, (b) insolation of $\text{PV}_1 = 100\%$ and insolation of $\text{PV}_2 = 80\%$, magnified version of v_{pv1}, v_{pv2}, v_{co1}, v_{co2} when (c) insolation of $\text{PV}_1 = 40\%$ and insolation of $\text{PV}_2 = 80\%$, (d) insolation of $\text{PV}_1 = 100\%$ and insolation of $\text{PV}_2 = 80\%$, magnified version of i_{L1}, i_{L2} when (e) insolation of $\text{PV}_1 = 40\%$ and insolation of $\text{PV}_2 = 80\%$, and (f) insolation of $\text{PV}_1 = 100\%$ and insolation of $\text{PV}_2 = 80\%$.

figures, Fig. 12(a) and (b), ensure that i_g remains to be sinusoidal and in-phase with v_g in spite of having difference in the magnitude of power being extracted from the two subarrays. From Fig. 12(c), it can be inferred that the converter associated with PV_1 operates completely in buck mode, whereas the converter associated with PV_2 operates in both buck and boost mode,

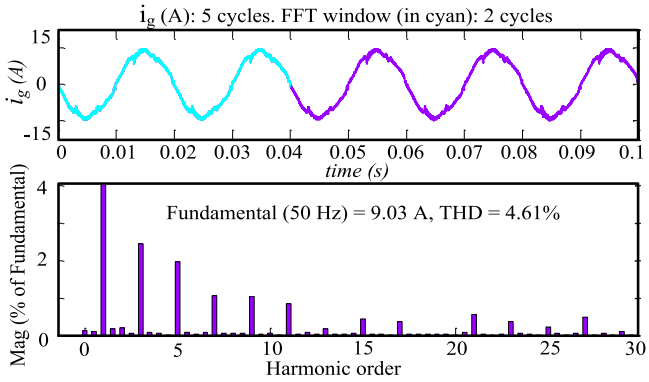

Fig. 13. Experimental waveform. FFT of i_g.

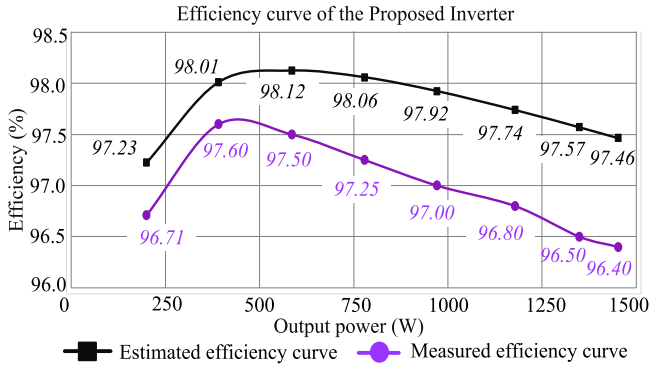

Fig. 14. Efficiency curves of the proposed inverter.

depending on the requirement. Thus, it can be inferred that the two converter segments are able to operate in a decoupled fashion. The measured variables, I_{pv1}, I_{pv2}, P_{pv1}, P_{pv2}, $V_{\text{co1}m}$, $V_{\text{co2}m}$, I_{gm}, I_{L1m}, and I_{L2m}, as depicted in Figs. 11 and 12, are more or less same as that of the estimated ones presented in Table III, and this validates the ability of the proposed inverter to extract maximum power from two subarrays operating under MEC.

Fig. 13 depicts the fast Fourier transform (FFT) of i_g. The THD of i_g is found to be 4.61%, which is below the limit of 5%, as specified in the standards, IEEE 1574/IEC 61727 [22]. It may be noted that the measured THD of v_g is found to be 2.12%, and hence, the contribution to THD from the inverter is much less than 4.61%.

The measured and estimated efficiency curves of the proposed inverter are shown Fig. 14. In order to measure the efficiency of the proposed inverter the Yokogawa make power analyzer, WT1800 is used and further, the losses incurred in the active and passive elements of the power circuit is considered while the losses involved with the control circuit are neglected. The efficiency is determined while both V_{pv1} and V_{pv2} are set at 130 V. Measured peak efficiency is found to be 97.65% and the measured European efficiency (η_{euro}) is obtained as 97.02%.

In order to measure the leakage current involved with the proposed inverter, 0.1 μF polypropylene film capacitors are used to emulate C_{pv1} and C_{pv2}. Fig. 15 depicts the voltages that appear

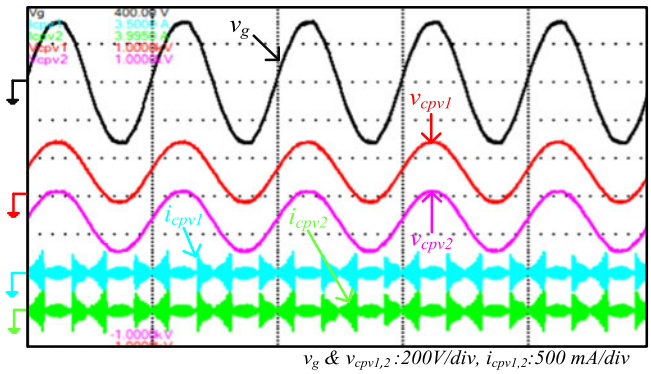

Fig. 15. Experimental waveform. v_g, v_{cpv1}, v_{cpv2}, i_{cpv1}, i_{cpv2}.

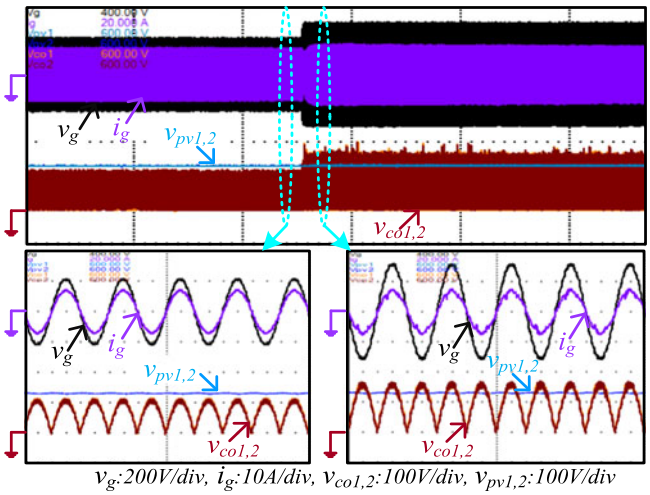

Fig. 16. Experimental waveform. v_g, i_g, v_{co1}, v_{co2}, v_{pv1}, v_{pv2} when v_g is changed from 150 V to 220 V.

across C_{pv1} and C_{pv2}, and the leakage currents, i_{cpv1} and i_{cpv2} flowing through C_{pv1} and C_{pv2}. The measured waveforms of v_{cpv1} and v_{cpv2} show that they contain significant amount of dc and low-frequency components whereas presence of high-frequency components are negligible. The measured rms value of total leakage current is found to be 80.7 mA, which is much lower than the limit 300 mA as specified in the standard, VDE 0126-1-1, and also cited in [23].

In order to demonstrate the stability of the proposed scheme in the event of a disturbance in v_g, a step change of 70 V (150–220 V) is introduced in v_g while V_{pv1} and V_{pv2} are kept at 130 V, and the references for the current controllers are purposely set at a fixed value in each mode. The response of the system during the aforesaid test condition where mode of operation of the proposed inverter is shifted from buck mode to buck and boost mode is shown in Fig. 16. It can be inferred from the Fig. 16 that the system can effectively ride through situations arising due to the disturbances in v_g.

A comparison of various features of the proposed scheme with existing transformerless schemes such as NPC-based scheme [5], H-Bridge-based scheme [2], schemes presented in [18] and [21] has been performed and presented in Table IV. Following issues are considered for carrying out this comparison.

1) Solar modules, i.e., Canadian solar "CS6P-165PE" [25], are utilized for the purpose.
2) Minimum input voltage requirement for NPC-based scheme [5] and H-Bridge-based scheme [2] is taken to be 800 V and 400 V, respectively, while minimum input voltage requirement of the schemes presented in [18] and [21] and that of the proposed scheme is taken to be 230 V.
3) For simplicity, total area required for a system is determined by multiplying the total number of modules required with the area of a single module.

The nomenclature used in Table IV is defined as follows: N_{PVR} = required number of PV arrays/subarrays, N_{PVC} = number of PV arrays controlled simultaneously, V_{IN} = input voltage requirement, N_{MS} = number of modules connected in series in a PV string of a PV array/subarray, which is made with a single string, N_{MT} = minimum number of modules required to design the PV system, P_{SYS} = minimum power rating of the PV system, A_{PV} = minimum area required to install all PV modules, E_{MEC} = possibility to get affected by MEC, which is determined from Table V. Based on the objective comparison presented in the Table IV it can be inferred that the proposed inverter deals with MEC in the most effective way.

In order to compare the power extraction from PV array by various transformerless schemes as mentioned in Table IV while

TABLE IV
COMPARISON TABLE OF VARIOUS TRANSFORMERLESS SCHEMES

Schemes	N_{PVR} and N_{PVC}	V_{IN} (V)	N_{MS} and N_{MT}	P_{SYS} (kW)	A_{PV} (m^2)	E_{MEC}
NPC based [5]	1 and 1	$>2V_m$	28 and 28	4.6	44.8	Highest
H-Bridge based [2]	1 and 1	$>V_m$	14 and 14	2.3	22.4	High
Reported in [18]	2 and 2	$<V_m$	8 and 16	2.6	25.6	Low
Reported in [21]	1 and 1	$<V_m$	8 and 8	1.3	12.8	Low
Proposed DBBI	2 and 2	$<V_m$	4 and 8	1.3	12.8	Lowest

TABLE V
EFFECT OF MEC IN DIFFERENT TRANSFORMERLESS SCHEMES

Schemes	Mod_{1in} (%) / P_{avl} (kW)	100 / 5.3	90 / 5.27	80 / 5.25	70 / 5.24	60 / 5.22	50 / 5.2
NPC based [5]	P_{ext} (kW)	5.3	5.2	4.9	4.53	4.1	3.6
	P_{diff} (kW)	0	0.07	0.35	0.71	1.12	1.6
	P_{lost} (%)	0	1.3	6.7	13.5	21.7	31.5
H-Bridge based [2]	P_{ext} (kW)	5.3	5.23	5.04	4.8	4.54	4.25
	P_{diff} (kW)	0	0.04	0.21	0.44	0.68	0.95
	P_{lost} (%)	0	0.8	4	8.2	13.1	18.3
Reported in [18]	P_{ext} (kW)	5.3	5.25	5.15	5.03	4.90	4.75
	P_{diff} (kW)	0	0.02	0.1	0.21	0.32	0.45
	P_{lost} (%)	0	0.4	2	4	6.1	8.6
Reported in [21]	P_{ext} (kW)	5.3	5.25	5.15	5.03	4.90	4.75
	P_{diff} (kW)	0	0.02	0.1	0.21	0.32	0.45
	P_{lost} (%)	0	0.4	2	4	6.1	8.6
Proposed DBBI	P_{ext} (kW)	5.3	5.26	5.21	5.14	5.08	5.01
	P_{diff} (kW)	0	0.01	0.04	0.1	0.14	0.19
	P_{lost} (%)	0	0.2	0.8	2	2.7	3.6

the schemes are operating under MEC, a 5.3 kW PV system at STC, built with 32 "CS6P-165PE" Canadian solar modules [25] is considered. Depending on the minimum dc voltage requirement, type of input connection required and power rating of the schemes, required number of PV modules are connected in series-parallel combination to form PV array/subarrays. The PV arrays/subarrays of the schemes are configured as follows:

1) $N_{\mathrm{MS}} = 32$ in [5];
2) $N_{\mathrm{MS}} = 16$ and $N_{\mathrm{MP}} = 2$ in [2], wherein N_{MP} = number of strings connected in parallel in an array/subarray;
3) $N_{\mathrm{MS}} = 8$ and $N_{\mathrm{MP}} = 2$ in [18];
4) $N_{\mathrm{MS}} = 8$ and $N_{\mathrm{MP}} = 4$ in [21];
5) $N_{\mathrm{MS}} = 4$ and $N_{\mathrm{MP}} = 4$ in DBBI.

Further, it is also assumed that no parallel diode is connected across PV modules. The insolation level of one module, $\mathrm{Mod}_{1\,\mathrm{in}}$ is varied from 100% to 50% with a step of 10% while the insolation of rest of the 31 modules are kept at 100%, i.e., at STC. The total estimated extracted power from the PV subarrays during MEC by any scheme, P_{ext} = power of affected string + power of rest of the string, the actual available maximum power in the PV array of any scheme, $P_{\mathrm{avl}} = 31\times$ power of each module + power of affected module, their difference, P_{diff} and the percentage loss of power due to MEC in any scheme, P_{lost} are tabulated in Table V. As the effect of MEC is less severe in parallel connected PV strings, the aforementioned effect is neglected to avoid complexity in calculation. From Table V it can be concluded that the proposed inverter is the most effective solution in extracting power during MEC.

VIII. Conclusion

A single phase GCT buck and boost based PV inverter that can operate two subarrays at their respective MPP was proposed in this paper. The attractive features of this inverter were as follows.

1) The effect of MECs on the PV array could be dealt with in an effective way.
2) The operating efficiency achieved, $\eta_{\mathrm{euro}} = 97.02\%$ was high.
3) Decoupled control of component converters was possible.
4) A simple MPPT algorithm was employed to ensure MPP operation for the component converters.
5) Leakage current associated with the PV arrays was within the limit mentioned in VDE 0126-1-1.

Mathematical analysis of the proposed inverter leading to the development of its small signal model was carried out. The criterion to select the values of the output filter components was presented. The scheme was validated by carrying out detailed simulation studies, and subsequently, the viability of the scheme was ascertained by carrying out thorough experimental studies on a 1.5 kW prototype of the inverter fabricated for the purpose.

References

[1] T. Shimizu, O. Hashimoto, and G. Kimura, "A novel high-performance utility-interactive photovoltaic inverter system," *IEEE Trans. Power Electron.*, vol. 18, no. 2, pp. 704–711, Mar. 2003.

[2] S. V. Araujo, P. Zacharias, and R. Mallwitz, "Highly efficient single-phase transformerless inverters for grid-connected photovoltaic systems," *IEEE Trans. Ind. Electron.*, vol. 57, no. 9, pp. 3118–3128, Sep. 2010.

[3] B. Ji, J. Wang, and J. Zhao, "High-efficiency single-phase transformerless PV H6 inverter with hybrid modulation method," *IEEE Trans. Ind. Electron.*, vol. 60, no. 5, pp. 2104–2115, May 2013.

[4] R. Gonzalez, E. Gubia, J. Lopez, and L. Marroyo, "Transformerless single phase multilevel-based photovoltaic inverter," *IEEE Trans. Ind. Electron.*, vol. 55, no. 7, pp. 2694–2702, Jul. 2008.

[5] H. Xiao and S. Xie, "Transformerless split-inductor neutral point clamped three-level PV grid-connected inverter," *IEEE Trans. Power Electron.*, vol. 27, no. 4, pp. 1799–1808, Apr. 2012.

[6] A. Bidram, A. Davoudi, and R. S. Balog, "Control and circuit techniques to mitigate partial shading effects in photo voltaic arrays," *IEEE J. Photovolt.*, vol. 2, no. 4, pp. 532–546, Oct. 2012.

[7] N. D. Kaushika and N. K. Gautam, "Energy yield simulations of interconnected solar PV arrays," *IEEE Trans. Energy Convers.*, vol. 18, no. 1, pp. 127–134, Mar. 2003.

[8] H. Patel and V. Agarwal, "Maximum power point tracking scheme for PV systems operating under partially shaded conditions," *IEEE Trans. Ind. Electron.*, vol. 55, no. 4, pp. 1689–1698, Apr. 2008.

[9] D. Nguyen and B. Lehman, "An adaptive solar photovoltaic array using model-based reconfiguration algorithm," *IEEE Trans. Ind. Electron.*, vol. 55, no. 7, pp. 2644–2654, Jul. 2008.

[10] G. Velasco-Quesada, F. Guinjoan-Gispert, R. Pique-Lopez, M. Roman-Lumbreras, and A. Conesa-Roca, "Electrical PV array reconfiguration strategy for energy extraction improvement in grid-connected PV systems," *IEEE Trans. Ind. Electron.*, vol. 56, no. 11, pp. 4319–4331, Nov. 2009.

[11] L. F. L. Villa, T.-P. Ho, J.-C. Crebier, and B. Raison, "A power electronics equalizer application for partially shaded photovoltaic modules," *IEEE Trans. Ind. Electron.*, vol. 60, no. 3, pp. 1179–1190, Mar. 2013.

[12] P. Sharma and V. Agarwal, "Maximum power extraction from a partially shaded PV array using shunt-series compensation," *IEEE J. Photovolt.*, vol. 4, no. 4, pp. 1128–1137, Jul. 2014.

[13] N. Femia, G. Lisi, G. Petrone, G. Spagnuolo, and M. Vitelli, "Distributed maximum power point tracking of photovoltaic arrays: Novel approach and system analysis," *IEEE Trans. Ind. Electron.*, vol. 55, no. 7, pp. 2610–2621, Jul. 2008.

[14] C. Olalla, C. Deline, D. Clement, Y. Levron, M. Rodriguez, and D. Maksimovic, "Performance of power-limited differential power processing architectures in mismatched PV systems," *IEEE Trans. Power Electron.*, vol. 30, no. 2, pp. 618–630, Feb. 2015.

[15] E. Karatepe, T. Hiyama, M. Boztepe, and M. Çolak, "Voltage based power compensation system for photo voltaic generation system under partially shaded insolation conditions," *Energy Convers. Manage.*, vol. 49, pp. 2307–2316, Aug. 2008.

[16] A. A. Elserougi, M. S. Diab, A. M. Massoud, A. S. Abdel-Khalik, and S. Ahmed, "A switched PV approach for extracted maximum power enhancement of PV arrays during partial shading," *IEEE Trans. Sustain. Energy*, vol. 6, no. 3, pp. 767–772, Jul. 2015.

[17] I. Patrao, G. Garcera, E. Figueres, and R. Gonzalez-Medina, "Grid-tie inverter topology with maximum power extraction from two photovoltaic arrays," *IET Renewable Power Gener.*, vol. 8, no. 6, pp. 638–648, Aug. 2014.

[18] D. Debnath and K. Chatterjee, "Maximising power yield in a transformerless single phase grid connected inverter servicing two separate photovoltaic panels," *IET Renewable Power Gener.*, vol. 10, no. 8, pp. 1087–1095, 2016.

[19] N. A. Ahmed, H. W. Lee, and M. Nakaoka, "Dual-mode time-sharing sine wave-modulation soft switching boost full-bridge one-stage power conditioner without electrolytic capacitor DC link," *IEEE Trans. Ind. Appl.*, vol. 43, no. 3, pp. 805–813, May/Jun. 2007.

[20] Z. Zhao, M. Xu, Q. Chen, J. S. Lai, and Y. Cho, "Derivation, analysis, and implementation of a Boost–Buck converter-based high-efficiency PV inverter," *IEEE Trans. Power Electron.*, vol. 27, no. 3, pp. 1304–1313, Mar. 2012.

[21] W. Wu, J. Ji, and F. Blaabjerg, "Aalborg inverter a new type of buck in buck, boost in boost grid-tied inverter," *IEEE Trans. Power Electron.*, vol. 30, no. 9, pp. 4784–4793, Sep. 2015.

[22] R. Teodorescu, M. Liserre, and P. Rodriguez, *Grid Converters for Photovoltaic and Wind Power Systems*. Hoboken, NJ, USA: Wiley, 2011.

[23] W. Li, Y. Gu, H. Luo, W. Cui, X. He, and C. Xia, "Topology review and derivation methodology of single phase transformerless photovoltaic inverters for leakage current suppression," *IEEE Trans. Ind. Electron.*, vol. 62, no. 7, pp. 4537–4551, Jul. 2015.

[24] W. Wu, Y. He, and F. Blaabjerg, "An LLCL power filter for single-phase grid-tied inverter," *IEEE Trans. Power Electron.*, vol. 27, no. 2, pp. 782–789, Feb. 2012.
[25] *Information on Canadian solar module CS6P-165PE*. [Online]. Available: www.solarhub.com/product-catalog/pv-modules/124

Subhendu Dutta was born in West Bengal, India. He received the B.Tech. degree in electrical engineering from West Bengal University of Technology, Kolkata, India, in 2009 and the M.E. degree in electrical engineering from Jadavpur University, Kolkata, India, in 2012. He is currently working toward the Ph.D. degree in the area of power electronics in the Department of Electrical Engineering, Indian Institute of Technology Bombay, Mumbai, India.

He worked as an Assistant Professor in the College of Engineering and Management, Kolaghat, India, from 2012 to 2013. His current research interests include the shading effect on solar photo voltaic systems, the design and efficiency improvement of power electronic converters for solar photovoltaic applications, and the design of magnetic elements for power electronic systems.

Kishore Chatterjee (M'10) was born in Calcutta, India, in 1967. He received the B.E. degree from Maulana Azad National Institute of Technology, Bhopal, India, in 1990; the M.E. degree from Indian Institute of Engineering Science and Technology, Howrah, India, in 1992, both in electrical engineering; and the Ph.D. degree from the Indian Institute of Technology (IIT) Kanpur, Kanpur, India, in 1998.

From 1997 to 1998, he was a Senior Research Associate with the IIT Kanpur. Since 1998, he has been with the Department of Electrical Engineering, IIT Bombay, Mumbai, India, where he is currently a Professor. He was a Visiting Fellow with École de Technologie Supérieure, University of Quebec, Montreal, QC, Canada, in 2004. He has been leading the power electronic group of the National Centre for Photovoltaic Research and Education, hosted with IIT Bombay, since 2009. His current research interests are power evacuation strategies from solar photovoltaic systems, modern VAR compensators, active power filters, utility-friendly converter topologies, and induction motor drives.